A Mass-Catcher for Large-Scale Lunar Material Transport

T. A. Heppenheimer*
Center for Space Science, Fountain Valley, Calif.

The large-scale transport of lunar mass, to supply resources for use in space colonization, may be accomplished via launch of small mass packages from the Moon by a mass-driver, onto ballistic trajectories, thus producing a mass-stream. This stream is caught by a mass-catcher – a powered vehicle which follows an optimized trajectory near the L2 libration point. Optimal mass-catching trajectories are found as solutions to a linear quadratic two-point boundary value problem, in which realistic operational conditions are incorporated in the equations of motion of the catcher. Direct use of the Maximum Principle, with no constraints on the initial or final state vectors, leads to optimal trajectories having unfavorably high initial and final velocities. By fixing these velocities under operational restrictions, the Maximum Principle permits study of a class of constrained optima. Catcher trajectories are rendered periodic by inclusion of a ballistic coast arc between terminal points. Required power levels and mission abort considerations are treated as functions of launch site longitude, and it is found that an admissible range of launch sites includes Tranquillity Base. A theory of mass-catching is proposed, based on results taken from the geologic theory of lunar cratering, and a reference catcher design is proposed.

Introduction

IN space colonization, one is concerned with the large-scale transport of lunar resources. The conceptual transport method receiving the most attention[1-3] involves a mass-driver (tracked electromagnetic accelerator) which launches a stream of small payloads on ballistic trajectories toward the L2 (translunar) libration point. There they are caught and consolidated for shipment.

The ballistic nature of the payload trajectories raises the question of arrival sensitivity to errors in launch velocity V_T. Let Δy be the miss distance from a nominal arrival point near L2, and ϵ the error in V_T. In general, the sensitivity is $\Delta y/\epsilon$ and is quite high[2]: $\Delta y > 1000$ km for $\epsilon = 1$ m/s. But it was discovered in 1976[2] that there is a focusing effect for trajectories in rotating coordinate systems; this effect can make Δy proportional not to ϵ but to ϵ^2. Then, for example, $\epsilon = 10$ cm/s gives $\Delta y = 20$ m.[3] Trajectories which achieve this focusing are known as "achromatic."

As conceived here, the mass-catcher is a powered vehicle which moves in space so as to always be reachable via achromatic trajectories from the mass-driver. This requirement involves theoretical considerations[3] which lead to the concept of the focus locus – the locus of points, reachable at a given time via achromatic trajectories from a fixed lunar site. The focus locus is a line in three-dimensional space, each point of which is associated with a value of V_T. The present study treats optimized catcher trajectories, the catcher being constrained to follow the focus locus.

Catcher Motion – Preliminary Considerations

Due to lunar geometrical librations, the launch site suffers displacements in longitude and latitude with a period of nearly one month. The location of the focus locus shifts in response to these librations. For planar motion (ignoring librations in latitude), Fig. 1 shows three focus locus locations (dashed lines) in the circular restricted three-body problem. Following Refs. 2 and 3, the launch site is equatorial and at longitude $\lambda = \lambda_0 = 33.1$-deg E, thus producing a focus locus through L2. The shift with time of focus locus location is due to the effective shift $\Delta\lambda$ in launch site longitude:

$$\Delta\lambda \sim -2e_m \sin t + \Delta\lambda_0 \tag{1}$$

e_m = lunar eccentricity = 0.0549, and $\Delta\lambda_0$ = offset in launch site longitude from λ_0. In this paper, the usual restricted-problem normalizations are used: unit distance = 384,410 km, unit time = (lunar period)/2π = 104.362 h, unit velocity = 1023.17 m/s, unit acceleration = 0.00273 m/s.^{2}

The mass-stream gives rise to both a momentum flux on the catcher and to large variations in catcher mass. The fill rate is taken as $\dot{m} = m_f/2\pi$; m = catcher mass, m_f = mass at the end of a fill cycle (one month). Then $m = \dot{m}t$. Now define the catcher motion in rotating coordinates (x, y, z) with origin at L2, x parallel to the Earth-Moon line of centers and away from the Moon. The mass-stream produces a perturbing acceleration on the catcher with components a_x, a_y, a_z:

$$a_x, a_y, a_z = (1/t)\{(V_x - \dot{x}), (V_y - \dot{y}), (V_z - \dot{z})\} \tag{2a}$$

$$(V_x^2 + V_y^2 + V_z^2)^{1/2} = V = 0.259 + 3.13x + 0.89y \tag{2b}$$

V_x, V_y, V_z are components of mass-stream velocity; Eq. (2b) is derived in Ref. 3. For the catcher motion,

$$\ddot{x} - 2\dot{y} - (1+2C)x - a_x = F(t) \tag{3a}$$

$$\ddot{y} + 2\dot{x} - (1-C)y - a_y = G(t) \tag{3b}$$

$$\ddot{z} + Cz - a_z = H(t) \tag{3c}$$

$C = 3.19042$; F, G, H are accelerations due to onboard thrust.

Special cases of Eqs. (3) yield reference solutions which constitute limiting cases. Thus, let $\Delta\lambda_0 = 0$ and express the effect of shifts in the focus locus location as

$$y = y_{\max.} \cos(t + \delta_0) \qquad y_{\max.} = 2e_m x_{L2} \tag{4}$$

where δ_0 is a constant phase angle; no generality is lost by taking $\delta_0 = 0$. x_{L2} = Moon-to-L2 distance = 0.167833. Let $a_x = a_y = a_z = z = 0$, and take $F = A \sin t$, $G = B \cos t$, where A and B are to be determined. Then minimize J, the ΔV:

$$J = \int_0^{2\pi} (F^2 + G^2)^{1/2} dt = \int_0^{2\pi} [B^2 - (B^2 - A^2)\sin^2 t]^{1/2} dt \tag{5}$$

Received Aug. 8, 1977; revision received Feb. 17, 1978.

Index categories: Electric and Advanced Space Propulsion; Lunar and Interplanetary Trajectories; Spacecraft Dynamics and Control.

*Chief Scientist. Member AIAA.

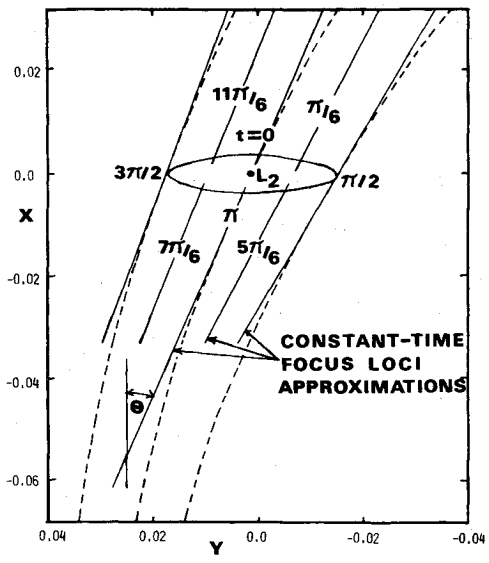

Fig. 1 Approximations to locations of a planar focus locus, and the solution of Eqs. (4) and (6). Unit time $t=104.362$ h, unit distance x, $y=384{,}410$ km.

and $J=4B\,E[(B^2-A^2)^{1/2}/B]$; $E(u)$ is the complete elliptic integral of the second kind. So J is minimized for $A=0$. Also,

$$x=[1/(C+1)]y_{\max.}\sin t \qquad B=y_{\max.}C(C-1)/(C+1) \quad (6)$$

and $J=4B=0.1227$ for the given values. The solution, Eqs. (4) and (6), is plotted in Fig. 1; the motion is retrograde.

To determine the monthly propellant expenditure required to follow this nominal path, it is convenient to refer the thrust components T_x, T_y, T_z to a full catcher; that is

$$T_x, T_y, T_z = (F,G,H)t/2\pi \quad (7)$$

which is simply Newton's second law. Then one defines ΔV_p:

$$\Delta V_P=\int_0^{2\pi}(T_x^2+T_y^2)^{1/2}\mathrm{d}t=2B \quad (8)$$

or 63.8 m/s per month. This is the "best case," where no propellant is required to counterbalance the mass-stream momentum flux. The propellant expenditure then is very nearly $m_f\Delta V_P/V_e$, to follow the nominal path; V_e is exhaust velocity.

A "worst case" exists if the catcher follows the indicated nominal path and, by continuous thrusting, nulls out the momentum flux. Thus, take $V=0.259$ [Eq. (2)] and $T_x=V/2\pi$; also take $T_y=\frac{1}{2}B\cos t$, corresponding to $m=m_f/2$. Then

$$\Delta V_P=2(B^2+4A^2)^{1/2}E[B(B^2+4A^2)^{-1/2}]=0.26771 \quad (9)$$

or 276.8 m/s per month.

The Catcher Equations

Now let the focus locus locations of Fig. 1 be approximated as straight lines whose angle to the x axis is $(\theta-\Delta\lambda)$; from Ref. 3, $\theta=-25.4588$ deg. One deals with a development of Eqs. (3), the linearized catcher equations.[3] These incorporate directly the lunar libration-induced shift in focus locus location, in both y and z coordinates, and include the effects of variable payload flight time as a function of location. Also included are all of the effects due to the mass-stream momentum flux upon a catcher of variable mass:

$$\ddot{x}+f_1(t)\dot{x}+f_2(t)x+f_3(t)=F(t) \quad (10a)$$

$$K\ddot{x}+g_1(t)\dot{x}+g_2(t)x+g_3(t)=G(t) \quad (10b)$$

$$P\ddot{x}+h_1(t)\dot{x}+h_2(t)x+h_3(t)=H(t) \quad (10c)$$

where

$$f_1(t)=1/t-2K$$

$$f_2(t)=-2\dot{K}-(1+2C)-(1/t)(3.13+0.89K)\cos(\theta-\Delta\lambda)$$

$$f_3(t)=-2\dot{D}-(1/t)(0.259+0.89D)\cos(\theta-\Delta\lambda)$$

$$g_1(t)=2\dot{K}+2+K/t$$

$$g_2(t)=\ddot{K}-(1-C)K+(1/t)[\dot{K}-(3.13+0.89K)\sin(\theta-\Delta\lambda)]$$

$$g_3(t)=\ddot{D}-(1-C)D+(1/t)[\dot{D}-(0.259+0.89D)\sin(\theta-\Delta\lambda)]$$

$$h_1(t)=2\dot{P}+P/t$$

$$h_2(t)=\ddot{P}+CP+(1/t)[\dot{P}-P(3.13+0.89K)]$$

$$h_3(t)=\ddot{Q}+CQ+(1/t)[\dot{Q}-P(0.259+0.89D)]$$

and where

$$K=(1+2e_m x_{L2}\sin\tau)\sin\theta+2e_m(\cos\tau-x_{L2}\sin\tau)+4e_m{}^2x_{L2}(\sin 2\tau-x_{L2}\sin^2\tau)+(1+4e_m x_{L2}\sin\tau)\Delta\lambda_0$$

$$D=2e_m x_{L2}(\cos\tau+e_m x_{L2}\sin 2\tau)+(1+2e_m x_{L2}\sin\tau)x_{L2}\Delta\lambda_0$$

$$P=-(\beta+\gamma\sin T)+2.285(0.2+0.078K)(\psi+\gamma\cos T)$$

$$Q=-x_{L2}(\beta+\gamma\sin T)+2.285(0.00851+0.078D)\times(\psi+\gamma\cos T)$$

The time variables are $\tau=t+\delta_0$ as in Eq. (4), $T=t+\delta_0+\phi$. ϕ circulates through 360 deg with period ~ 6 years, due to solar perturbations on the lunar orbit. In this paper, ϕ is fixed for a given problem. The lunar launch site is at latitude β, with the mass-stream launched north from due east by angle ψ. γ is the lunar obliquity, 6.7 deg. Equations analogous to Eq. (4) are

$$y=K(t)x+D(t) \qquad z=P(t)x+Q(t) \quad (11)$$

Equations (11) are derived in Ref. 3, as are the definitions of K, D, P, and Q. Equations (10) then follow from Eqs. (2, 3, and 11).

Return Trajectories

Consider optimized solutions of Eqs. (10), with fixed initial and final time. Final time t_f is 2π always. Initial time $t_0=(m_0/m_f)\ 2\pi$; $m_f/m_0=$ ratio of full-to-empty catcher mass.

This paper treats periodic catcher trajectories. Periodicity is achieved by designating the initial time interval, 0 to t_0, as a coast arc along which the catcher returns from (x_f, y_f, z_f) to (x_0, y_0, z_0), these locations being found from the optimization. It is convenient to regard this coast arc as an impulsive ballistic solution to the linearized equations of motion near L2. Following Nicholson,[4] at t_f one finds velocity components $\dot{X}_0$, $\dot{Y}_0$, $\dot{Z}_0$ satisfying

$$x_0=(1.3347x_f+0.2460\dot{Y}_0)\cosh s_1t_0-(0.2496y_f-0.3904\dot{X}_0)\sinh s_1t_0-(0.3347x_f+0.2460\dot{Y}_0)\cos s_2t_0+(0.2893y_f+0.0845\dot{X}_0)\sin s_2t_0 \quad (12a)$$

$$y_0 = -(0.8412x_f + 0.1551\dot{Y}_0)\sinh s_1 t_0 + (0.1573y_f - 0.2460\dot{X}_0)\cosh s_1 t_0 + (0.9749x_f + 0.7166\dot{Y}_0)\sin s_2 t_0 + (0.8427y_f + 0.2460\dot{X}_0)\cos s_2 t_0 \quad (12b)$$

$$z_0 = (\cos C^{1/2} t_0) z_f + C^{-1/2} \sin(C^{1/2} t_0)\dot{Z}_0 \quad (12c)$$

s_1, s_2 are eigenvalues: $s_1 = 2.15868$, $s_2 = 1.86265$. Equations (12a) and (12b) are linear in the unknowns $\dot{X}_0$, $\dot{Y}_0$. Here (x, y, z) refers to the thrust arc and (X, Y, Z) to the coast arc, the terminal point of each being the initial point of the other. Also, $\dot{X}_f$, $\dot{Y}_f$, $\dot{Z}_f$ (at $t = t_0$) are given by

$$\dot{X}_f = \partial x_0/\partial t_0 \qquad \dot{Y}_f = \partial y_0/\partial t_0 \qquad \dot{Z}_f = \partial z_0/\partial t_0 \quad (13)$$

and the total ΔV for the return maneuver is denoted ΔV_R:

$$\Delta V_R = (m_0/m_f)\{[(\dot{x}_0 - \dot{X}_f)^2 + (\dot{y}_0 - \dot{Y}_f)^2 + (\dot{z}_0 - \dot{Z}_f)^2]^{1/2} + [(\dot{x}_f - \dot{X}_0)^2 + (\dot{y}_f - \dot{Y}_0)^2 + (\dot{z}_f - \dot{Z}_0)^2]^{1/2}\} \quad (14)$$

The computation of ΔV_R would be improved by studying the return trajectories within a low-thrust optimization problem. But it will be seen that $\Delta V_R \ll \Delta V_P$; hence this refinement would not significantly change the overall mission requirements.

Optimal Solutions Without Constraints

Equations (10) involve the angle parameters δ_0, ϕ; hence it is convenient to simplify the initial studies by considering motion in the x-y plane, thus suppressing ϕ. Here $\Delta\lambda_0 = 0.01$, corresponding to the topographically suitable site closest to λ_0.[3] For simplicity, the optimization is formulated as a linear quadratic problem (LQP), which can be solved without iteration. Thus, define the control $u = \ddot{x}$ and the problem is stated:

Minimize

$$J = \int (\text{thrust})^2 dt$$

$$J(u, x, \dot{x}; t) = \int_0^{2\pi} (t/2\pi)^2 (F^2 + G^2)\, dt \quad (15)$$

where $F = F(u, x, \dot{x}; t)$ and $G = G(u, x, \dot{x}; t)$ under Eqs. (10). The integrand is $(T_x^2 + T_y^2 + T_z^2)$, Eq. (7), rather than $(T_x^2 + T_y^2 + T_z^2)^{1/2}$ as in Eq. (8), since the latter would not permit formulation as an LQP. The Maximum Principle gives:

The Hamiltonian

$$H = (t/2\pi)^2 (F^2 + G^2) + \Lambda_1 \dot{x} + \Lambda_2 u \quad (16)$$

The control equation

$$\partial H/\partial u = 0 \quad (17)$$

The equations of motion

$$dx/dt = \dot{x} \qquad d\Lambda_1/dt = -\partial H/\partial x$$

$$d\dot{x}/dt = u(x, \dot{x}; t) \qquad d\Lambda_2/dt = -\partial H/\partial \dot{x} \quad (18)$$

The transversality condition

$$(H dt - \Lambda_1 dx - \Lambda_2 d\dot{x})_{t_0}^{t_f} = 0 \quad (19)$$

In Eq. (16), Λ_1, Λ_2 are Lagrange multipliers. In Eq. (17), the fact that H is quadratic in u leads to a linear equation which permits eliminating u in favor of terms in x, $\dot{x}$, t, as noted in Eqs. (18). This elimination is the key feature of an LQP.

One considers a fixed-time problem for which no constraints are placed on initial or final values of x, $\dot{x}$. Hence, in Eq. (19), dx, $d\dot{x}$ are $\neq 0$ and the boundary conditions are given:

$$\Lambda_1(t_0) = \Lambda_2(t_0) = \Lambda_1(t_f) = \Lambda_2(t_f) = 0 \quad (20)$$

A solution then proceeds by integrating Eqs. (18) with arbitrary $x(t_0)$, $\dot{x}(t_0)$, and with $\Lambda_1(t_0) = \Lambda_2(t_0) = 0$, from t_0 to t_f. One then performs differential correction on $x(t_0)$, $\dot{x}(t_0)$ so as to drive $\Lambda_1(t_f)$, $\Lambda_2(t_f)$ to zero. In principle, this differential correction involves a linear function so that a single stage of Newton iteration produces convergence. But solutions to Eqs. (18) are unstable and, hence, sensitive to small changes in $x(t_0)$, $\dot{x}(t_0)$; the elements of $\partial[x(t_f), \dot{x}(t_f)]/\partial[x(t_0), \dot{x}(t_0)] = 10^6$ to 10^7. The computer used (a CDC 3300) could accommodate only 10 to 11 significant figures. The first Newton iteration reduced the errors in $\Lambda_1(t_f)$, $\Lambda_2(t_f)$ by up to six orders of magnitude. But it nevertheless was found convenient to repeat the Newton iteration up to three additional times. Typically, then, $|\Lambda_1(t_f)|$, $|\Lambda_2(t_f)|$ converged to 10^{-4} (for $m_f/m_0 = 5$) to 10^{-2} (for $m_f/m_0 = 50$). The associated errors in computed quantities, particularly ΔV_P, were 10^{-1} to 10^{-2} less, and the computed accuracies were regarded as acceptable. Integrations were performed with a sixth-order Runge-Kutta routine with a fixed time step, $\Delta t \sim 0.05$, the exact value being chosen so $(t_f - t_0)/\Delta t$ is an integer. No significant changes were found for Δt as small as ~ 0.005. During the final integrations, ΔV_P was computed as in Eq. (8).

Figure 2 gives parameters for unconstrained optima. In part 1, $m_f/m_0 = 15$; BC is the "best case," Eq. (8); WC is the "worst case," Eq. (9). Curve (a) is ΔV_P; (b) is ΔV_R. For the most favorable value of δ_0, ~ 315 deg, ΔV_P is close to BC. For this value of δ_0, part 2 of Fig. 2 gives ΔV_P, ΔV_R, $\Delta V_P + \Delta V_R$ as functions of m_f/m_0.

Figure 3 shows the periodic orbits of part 2 of Fig. 2. Ballistic return trajectories are dashed. As in Fig. 1, the motion is generally clockwise (retrograde); the sense of the return trajectories is the positive x direction. There is close similarly of the orbits for $m_f/m_0 \geq 15$, so only the initial points (x_0, y_0) are given for $m_f/m_0 = 15, 20, 30, 40$.

Initially the catcher descends rapidly toward the Moon, but below L2 its motion is checked by the mass-stream momentum flux. Thereafter it follows a looped trajectory

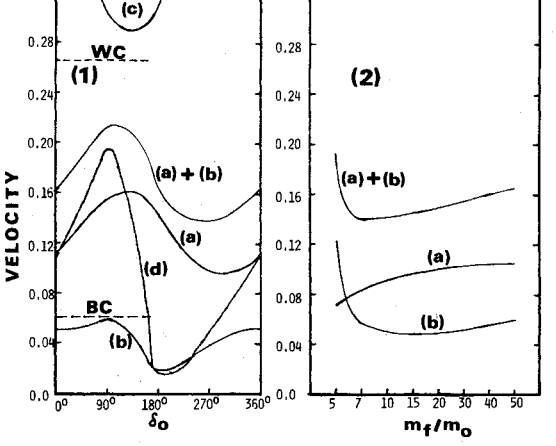

Fig. 2 Characteristics of unconstrained optima: part 1 (left), $m_f/m_0 = 15$; part 2 (right), $\delta_0 = 315$ deg. Curves: (a) ΔV_P; (b) ΔV_R; (c) $\dot{x} - V_x$ at $t = t_0$; (d) $\dot{x}_f$; BC, Eq. (8); WC, Eq. (9). Unit velocity = 1023.17 m/s.

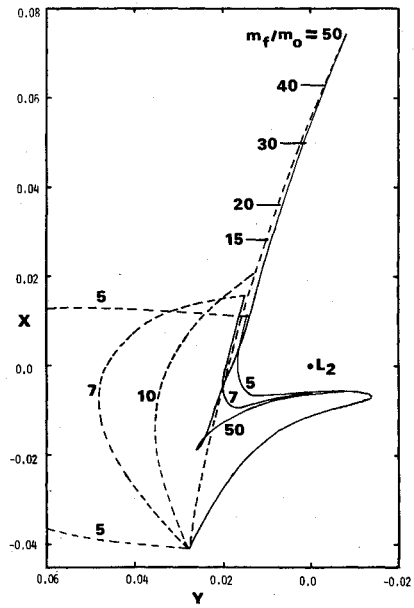

Fig. 3 Planar unconstrained optimal trajectories; thrust arcs are solid lines, coast arcs (return trajectories) are dashed. Parameters are as in part 2 of Fig. 2, x, y as in Fig. 1.

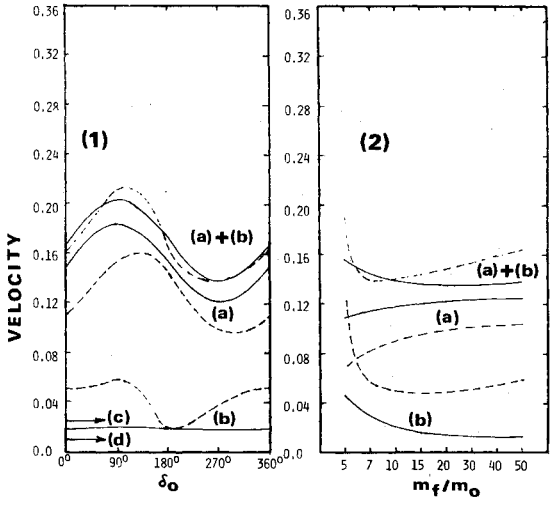

Fig. 4 Characteristics of operationally constrained planar optima: part 1, $m_f/m_0 = 15$; part 2, $\delta_0 = 270$ deg. Curves are as in Fig. 2; dashed curves from Fig. 2 with $\delta_0 = 315$ deg in part (2).

resembling the ellipse of Fig. 1, but displaced below L2. This displacement results from the loop being centered, not at L2, but at an equilibrium between the potential gradient and the acceleration due to the mass-stream, i.e., a dynamical libration point.[2] As the catcher approaches a full load, it relieves its thrust requirements by falling away from L2. The termination point is nearly invariant with m_f/m_0; indeed, this invariance serves as a test of computation accuracy.

Such trajectories possess unfavorable operational characteristics, as shown in Fig. 2. Curve (c) gives the initial impact velocity, $V_x - \dot{x}$, at $t = t_0$. The high values pose risk of damage. Also, curve (d), nearly invariant as a function of m_f/m_0, gives $-\dot{x}_f$. Since a fully loaded catcher cannot readily be maneuvered, curve (d) approximates the x component of the release velocity – the velocity of the consolidated material as it starts its way toward the colony. Yet, as discussed elsewhere,[5] it is desirable to have $\dot{x}_f \sim -0.01$. Finally, the requirement for reversal of the motion at t_0, and to a lesser extent at t_f, lead to high values of ΔV_R. Thus, consider a class of optimized solutions involving constraints characteristic of actual mission operations.

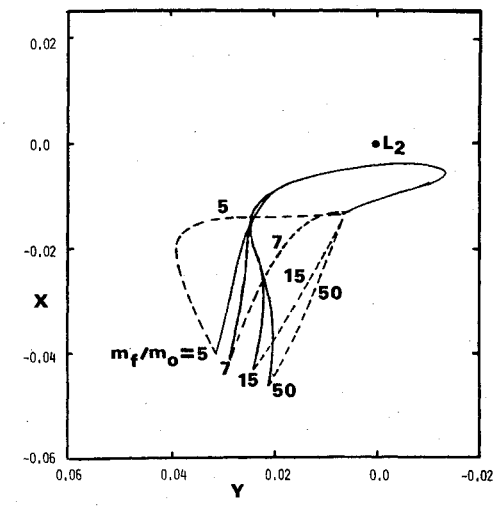

Fig. 5 Planar operationally constrained optimal trajectories. Parameters are as in part 2 of Fig. 4. x, y are as in Fig. 1.

Operationally Constrained Optimal Solutions

At $t = t_0$, let $V_x - \dot{x} = 0.025$; at $t = t_f$, $\dot{x} = -0.01$. The first of these reflects a desire to reduce the initial impact velocity by an order of magnitude from the values of Fig. 2; the second reflects considerations of release velocity. The optimization then involves Eqs. (15-18) which are unchanged; but Eq. (19) gives rise to new boundary conditions:

$$\dot{x}(t_0) = V_x(x;t_0) - 0.025 \tag{21a}$$

$$\Lambda_2(t_0) = \Lambda_2(t_f) = \dot{x}(t_f) + 0.01 = 0 \tag{21b}$$

In Eq. (21a), $V_x = V_x(x;t_0)$ is found from Eqs. (1, 2, 10, and 11). Solution then consists of Newton iteration on $x(t_0)$, $\Lambda_1(t_0)$ so as to drive $\Lambda_2(t_f)$, $\dot{x}(t_f) + 0.01$ to zero.

Figure 4 then is the counterpart of Fig. 2; dashed curves are from Fig. 2 for comparison. The constrained problem produces a modest increase in ΔV_P, but ΔV_R is substantially reduced, so there is little change in the sum. Again, in part 1, $m_f/m_0 = 15$, in part 2, $\delta_0 = 270$ deg for the solid curves and 315 deg for the dashed curves, δ_0 being chosen to minimize ΔV_P.

Figure 5 is the counterpart of Fig. 3. ΔV_R is reduced because the trajectories are more compact and have smoother transitions into the return trajectories at t_f. Again, the motion is generally clockwise. Comparison of Figs. 5 and 3 shows little change in the looped portions of the thrust arcs. The catcher does not descend so far from L2 in Fig. 5, since this would violate the $\dot{x}(t_f)$ constraint; the major difference between the two figures involves the initial portions of the thrust arcs. Yet, these changes produce little change in ΔV_P (Fig. 4).

Hence one may constrain the initial catcher motion (say, from t_0 to $t_0 + t_f/10$) by operational conditions such as low impact velocity, and there is little change in ΔV_P. Major changes in ΔV_P are expected only if one seriously disturbs the looped portion of the trajectory, which appears as a general feature of optimal catcher trajectories.

In particular, suppose that the initial portion of the thrust arc is to be constrained by a requirement such as

$$(\dot{x}^2 + \dot{y}^2)^{1/2} - V(x;t) = \Delta V(t) \tag{22}$$

$\Delta V(t)$ is a specified time function and $V = V(x;t)$ follows from Eqs. (2, 10, and 11). This gives a quadratic equation in $\dot{x}$ from which $\dot{x} = \dot{x}(x;t)$. Hence, in Eqs. (10), one eliminates $\dot{x}$, $\ddot{x}$ in favor of terms in x, t. In optimization, the control $u = x$ and, for the problem of Eq. (15), the Maximum Principle

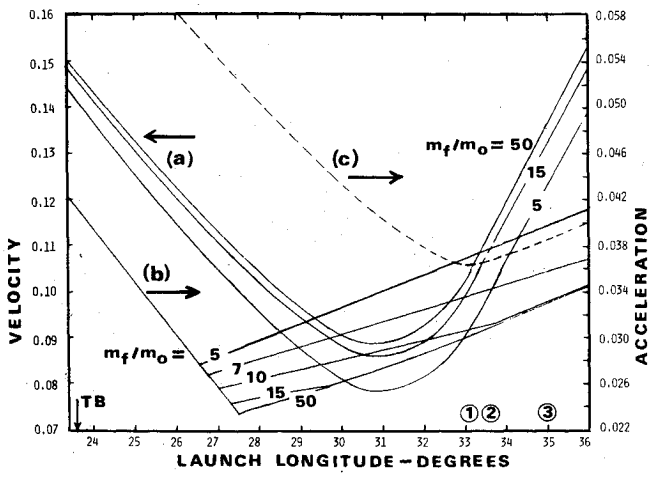

Fig. 6 Characteristics of operationally constrained optima as functions of λ_0; $\delta_\theta = 270$ deg. Curves: (a) ΔV_P (unity = 1023.17 m/s); (b) maximum nominal thrust (unity = 0.00273 m/s^2 $\times m_f$ in kg); (c) maximum emergency (abort) thrust.

reduces to

$$\frac{\partial}{\partial u}\left[F^2(u;t)+G^2(u;t)\right]=0 \tag{23}$$

So this portion of the thrust arc is defined by an algebraic equation, not by a two-point boundary value problem.

Launch Site Location Considerations

Launch site location effects were studied by taking $\Delta\lambda_0$ in the range, -0.17 to $+0.05$ rad. For each such launch site and for $\delta_0 = 270$ deg, the optimization of Eqs. (15-18, 21) was performed. The results are in Fig. 6.

Curve (a) is ΔV_P, for three values of m_f/m_0; ΔV_R is not plotted because it is essentially as in Fig. 4. ΔV_P is influenced strongly by the mass-stream momentum flux, which is at the angle $(\theta-\Delta\lambda)$ to the x axis. The resulting y component of momentum flux moves the minimum in ΔV_P from $\lambda_0 = 33.1$ deg to $\lambda = 30.7$ deg. For launches from more westerly locations, the continuing decrease in $\Delta\lambda_0$ produces a dynamical libration point which shifts ever further in the negative y direction, thus ameliorating the increase in ΔV_P. This effect extends as far westward as Tranquillity Base (TB). But for launch sites east of λ_0, ΔV_P increases rapidly because the dynamical libration point remains east of the x axis.

Curves (b) give maximum thrust, Eq. (7). Many of the computed thrust/time curves showed large (~ 0.10) values of thrust for t near t_0. Since this involves the portion of the thrust arc which is most readily modified, it was arbitrarily assumed that a thrust-limitation constraint may be applied between t_0 and $t_0 + t_f/10$ so that the plotted thrust values are the maxima in the range, $(t_0 + t_f/10)$ to t_f. Many of the thrust/time curves showed two local maxima. The envelope of curves (b), Fig. 6, then is the larger of these two; this envelope was nearly invariant with m_f/m_0. But the upward-sloping labelled curves are associated with a third maximum: the value at $t = t_0 + t_f/10$. Such curves then are artifacts of the adopted model.

In principle, one may define power and thrust requirements from curves (b), propellant-mass requirements from curve (a). But one must consider operational catcher abort. Such an abort would occur in the event of interruption of the mass-stream, e.g. due to shutdown of the mass-driver at the Moon, or loss by the catcher of the focus locus. The abort mode treated here is that the catcher continues to follow its computed nominal path, e.g., Fig. 5, pending reacquisition of the mass-stream. During this time its thrust requirements are defined as solutions to Eqs. (3) wherein x, y, z are known time functions and $a_x = a_y = a_z = 0$. Curve (c), dashed for clarity, which is also virtually invariant with m_f/m_0, defines the maximum thrust which may be required in such an abort, again following Eq. (7). This curve does reach its minimum at $\lambda = \lambda_0$. Note that abort could require less power or maximum thrust than would normal mission operations.

In Fig. 6, TB is Tranquillity Base; point 1 is λ_0; point 2 is the adjacent mare site used in this paper. Point 3 is of interest because payloads launched from that site could pass either of two mountains downrange.

Such downrange mountains may serve to increase launch accuracy. Chilton et al.[6] have suggested establishing corrector stations on such mountains, some 50 km, or 20 s of flight time, downrange. Launch velocity errors then yield position errors which may be detected so as to indicate the magnitude of required adjustment to launch velocity components.

Using achromatic trajectories, the most sensitive velocity component is associated with errors in the y direction (V_N); for an admissible error in y of ± 50 m at the catcher, $\Delta V_N \leq 0.001$ m/s. A 20-s flight then gives a position error of 2 cm. For spherical payloads, such a position error is detectable by causing each payload to occult a pair of point light sources and timing the occultations, as in a stellar occultation in planetary astronomy. Chilton et al.[6] propose detection of errors < 0.1 cm by this method. Hence the payload dispersion at the catcher may be > 20 times better than required, if the detected launch errors are corrected via the electrostatic-deflection method of Ref. 6.

This conclusion is not modified by gravitational perturbations since such perturbations do not prejudice the existence of achromatic trajectories, but merely modify the shape and location of the focus locus.[3] But random nongravitational perturbations, due to payloads' interaction with the space environment, can produce a larger dispersion. Such random effects would arise from variations in individual payloads' albedo, electric or magnetic properties, center-of-mass location, etc. Hence, appropriate control of payload manufacturing may achieve uniformity in these properties, and will eliminate significantly large random perturbations of this nature. Nongravitational perturbations on successive payloads then would not be random but would be correlated, and again the focus locus would merely be biased in shape and location.

The conclusion is that the catcher size may be driven, not by launch inaccuracies, but by the simple requirement that it provide sufficient volume for the caught mass.

Three-Dimensional Solutions

With $\delta_0 = 270$ deg, the full three-dimensional Eqs. (10) have been subjected to optimization under Eqs. (21). The launch site is again site 2 of Fig. 6: $\Delta\lambda_0 = 0.01$, and $\beta = 1.73$ deg. Also $\psi = 18.306$ deg; this value is optimal for the cited β.[3] But ϕ cannot be chosen at will since its value is determined by lunar perturbations. Thus, whereas previously ΔV_P and $\Delta V_P + \Delta V_R$ were to be minimized, now one must consider their maximum values, as functions of ϕ.

Figure 7 is the counterpart of Figs. 2 and 4. The dashed curves are reproduced for comparison from Fig. 4; in part 1 of Fig. 7, where $m_0/m_f = 15$, they are constant insofar as ϕ has no meaning for the planar case. The difference between corresponding dashed and solid curves represent effects attributable to three-dimensionality. The minimum velocity requirements occur approximately for $\phi = 225$ deg. Then with $\delta_0 = 270$ deg, $\phi = 225$ deg, part 2 of Fig. 7 gives ΔV_R, ΔV_P, $\Delta V_R + \Delta V_P$.

Because the y and z motions are completely constrained in consequence of the lunar librations, one expects the traces of the trajectories, in the y-z plane, to resemble Lissajous curves. This is confirmed in Fig. 8, which plots trajectories for $\delta_0 = 270$ deg, $m_f/m_0 = 15$ and for four values of ϕ. Arrows indicate the sense of the motion; ballistic-return trajectories are dashed. The trajectories are offset to the west of L2 owing

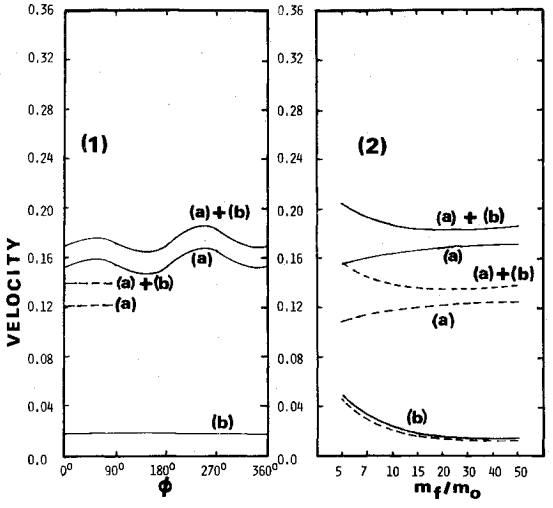

Fig. 7 Same as Fig. 4 except for operationally constrained three-dimensional optima; $\delta_0 = 270$ deg: part 1, $m_f/m_0 = 15$; part 2, $\phi = 225$ deg. Dashed curves reproduced from Fig. 4.

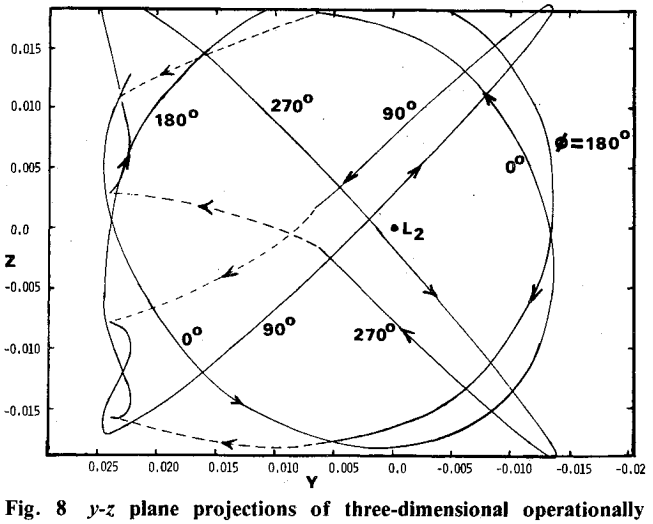

Fig. 8 y-z plane projections of three-dimensional operationally constrained optima. Parameters are as in part 1 of Fig. 7. Unit distance $y, z = 384{,}410$ km.

to the displacement of the launch site in $\Delta\lambda_0$. But the optimal choice of ψ renders them nearly symmetric about the z axis, despite the nonzero latitude β at launch.

Consider now the use of these data in obtaining information of engineering interest. Let $\delta_0 = 270$ deg, $\phi = 225$ deg, $m_f/m_0 = 15$. From Fig. 7, $\Delta V_P = 0.16566 = 169.50$ m/s. Also, $\Delta V_R = 0.01699 = 17.38$ m/s. If the loaded catcher has mass $m_f = 10^5$ tons, a typical value (1 ton $= 10^3$ kg), and if propulsion is by rotary pellet launchers (RPL's) of reference design,[1] with $I_{sp} = 405$ s, then the required propellant (pellets) is 4713 tons. Some 1% of this may represent tankage mass.

Figure 9 gives further data. "Emergency acceleration" is the thrust required in a mission abort. "Nominal acceleration" is the thrust required to follow a nominal path such as that of Figs. 5 and 8; this curve exhibits the three local maxima discussed in association with curves (b) of Fig. 6. Since an abort situation occurring near the end of the catching cycle may lead to payload-release operations rather than to efforts to resume catching, it appears reasonable to select the required thrust acceleration as $0.045 = 1.2285 \times 10^{-4}$ m/s^2; this permits nominal operations under a safety margin of $\geq$ 10%, while preserving an abort option for $\geq$90% of the catching cycle. Then, onboard thrust = 12,285 N and onboard power = 24.355 MW. The thrust is effectively provided by four reference RPL units at 17.34 tons each. If the onboard

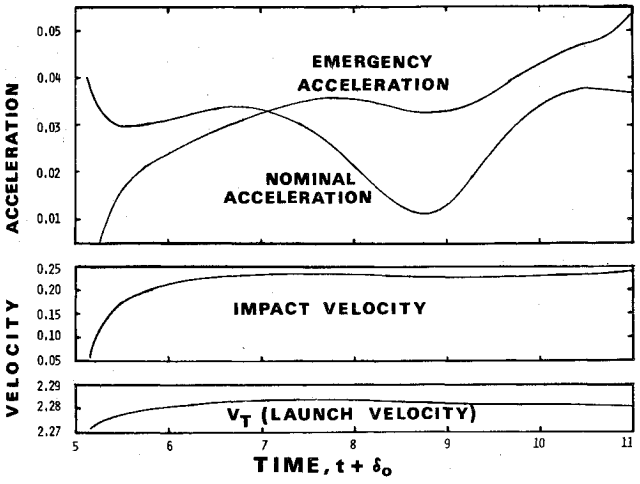

Fig. 9 Operational characteristics of a three-dimensional operationally constrained optimum: $\delta_0 = 270$ deg, $\phi = 225$ deg, $m_f/m_0 = 15$. Units are as in Figs. 1 and 6.

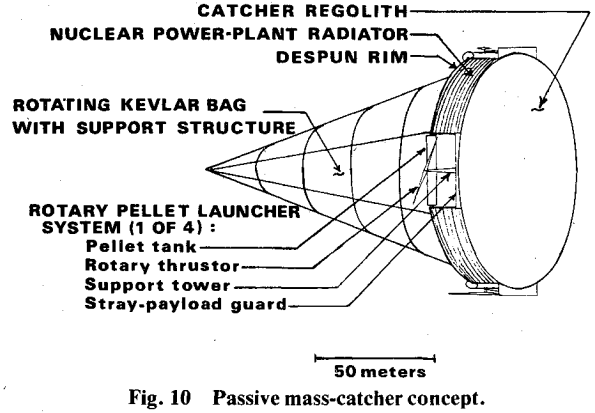

Fig. 10 Passive mass-catcher concept.

power is provided by a nuclear plant at a reference specific mass of 45 tons/MW,[1] its mass is 1096 tons.

Figure 9 also gives time histories of payload impact velocity, $V_i = [(V_x - \dot{x})^2 + (V_y - \dot{y})^2 + (V_z - \dot{z})^2]^{1/2}$ (see Eq. 2), and of launch velocity V_T. The former is of significance in design of the catcher systems which receive the impacts; in addition, the relatively rapid initial rise gives insight into the desirability of a constraint such as Eq. (22). A curve such as the latter is derived from (for example) Fig. 5, using the linearized correlation[3]

$$V_T = 2.285 + 0.375x + 0.095y \tag{24}$$

Moreover, such a curve is closely associated with catcher navigation. The nominal path is quite unstable. But a reference nominal path can be used to develop a nominal program for V_T. In practice, $V_T(t)$ will be measured to great accuracy at launch, and can be used to predict the required motion of the mass-catcher, such predictions being available for the duration of payload flight time (some 48 h).

Theory of Catching and Bag Design

Consider the physics of catching. A reference catcher concept involves a large conical bag[1] (Fig. 10). The caught material forms a layer of lunar soil over the inside of the bag; this layer is referred to as the catcher regolith (CR). A uniformly thick CR is achievable if the launch accuracies are high enough to give a mass-stream dispersion at the catcher which is much smaller than the catcher's dimensions.

For stable rotation of such a bag and CR, the axial moment of inertia must exceed the longitudinal moment. This is achievable for the aspect ratio, (length)/(aperture radius),

$L/R>3$. The resulting "slope" of the CR is 18.435 deg and since lunar soil resembles terrestrial sand, angle-of-repose considerations appear to permit a stable CR.

The impact of a payload into the CR produces a crater, which may damage the bag; and it produces ejecta, some of which may escape the catcher. Thus, let $Q(V_i,i)$ be the ratio between total mass of ejecta and mass of impacting payload, when the latter impacts at incidence angle i and velocity V_i. Let $G(\phi, V_e, V_i)$ be the fraction of ejecta with direction of motion between ϕ and $\phi+d\phi$ ($\phi=0$ deg is the direction of payload motion) and with velocity $V_{ej}\geq V_e$. Here V_e is not exhaust velocity, but is a reference ejection velocity.

Experimental data on G and Q are available from geological studies. However, virtually all such work has been done at hypervelocity ($V_i\gg 1$). Such impacts involve explosive energy release. At $V_i\ll 1$, the case here, one may expect significant effects due not only to energy release but also to momentum transfer from payload to CR material. At present there are few experimental data suitable for study of this.

However, one may use the hypervelocity data for preliminary assessment. It can be argued that this procedure is conservative. Thus, in hypervelocity cratering, $\partial G/\partial\phi=0$, i.e. the angular distribution of ejecta is uniform. At low V_i, one may expect $G(\phi=0 \text{ deg}, V_e, V_i)>G(\phi=180 \text{ deg}, V_e, V_i)$, i.e. there may be a concentration of ejecta in the forward direction. Such an effect would produce craters which are elongate rather than circular and which hence are shallower. Also, any tendency to eject material deeper into the bag obviously militates against its escaping the catcher.

For impacts into unbonded quartz sand, Marcus[7] gives

$$Q(V_i,i)=215V_i^2(\cos i)^{3/2} \tag{25}$$

and $\cos i=10^{-1/2}$ for an aspect ratio of 3. Overbeck et al.[8] gives the depth-to-diameter ratio of an impact crater in regolith as 0.26. Then if the crater in the CR is a segment of a sphere, its depth D is related to payload diameter P by

$$D=2.61PV_i^{2/3}(\cos i)^{2/9} \tag{26}$$

or, from Fig. 9, $D\sim 0.75P$ for the impact velocities given. It thus is possible to assess tradeoffs between payload design and aspects of catcher design; such considerations also may involve the mass-driver. For example, considerations of physical containment suggest a catcher aperture diameter $2R=100$ m for the concept of Fig. 10 and for a full load, 10^5 tons; such a load fills the bag out to some 60 m from the tip. This load then forms a CR of depth ~ 1.5 m, taking the density as 2.5 g/cm^3. If one uses proposed 20-kg payloads,[6] then one may require a CR depth of 19 cm before initiating high-velocity catching. Hence, the first 13% of the catching cycle may require a constraint such as Eq. (22), or else it may be necessary to modify the given geometrical factors.

Overbeck et al.[8] note that lunar crater ejecta fall within 7 crater radii of the impact site. Murray[9] notes that on Mercury, ejecta blankets form more closely due to the higher Mercurian gravity. So for any reasonable bag rotation rate, spillover effects producing major mass-loss should be negligible within a few payload-diameters of the rim. More specifically, let $G(\phi, V_e, V_i)=G(V_e, V_i)$, i.e. the distribution of ejecta is isotropic. Hypervelocity data appropriate to determination of $G(V_e,V_i)$ have been given by Gault et al. (see discussion by Marcus[7]) and suggest the following:

$$G=\min\{1, 10^{-4}(V_i/V_e)^2\} \tag{27}$$

since obviously $G\leq 1$.

Let the bag be rotating so as to produce a local velocity V_B at an impact site; V_B is normal to the catcher axis. Ejecta with $V_{ej}<V_B$ behave as in a gravity field and do not escape. Escape is possible for $V_{ej}>V_B$. It is assumed that, in fact, escape does occur for that fraction so ejected into a solid angle corresponding to that fraction of 2π steradians (one hemisphere) subtended by the aperture. This fraction is the area ratio $\mathcal{R}$.

Now let any station along the catcher length be at distance l from the tip, $l<L$. The catcher rotates so as to produce velocity $V_B=V_{BL}$ at the aperture; in general, $V_B=V_{BL}\cdot(l/L)$. $\mathcal{R}$ is approximately 1/2 at $l=L$, 1/18 at $l=0$. To find $\mathcal{R}$ at intermediate stations, consider that, approximately, $\mathcal{R}\propto l^2$; hence a useful expression is

$$\mathcal{R}=(1/18)[1+2(l/L)]^2 \tag{28}$$

The mass-loss fraction (MLF) = (fraction lost)/(total incident):

$$\text{MLF}=\int_0^l \mathcal{R}(l/L)\cdot G(V_B,V_i)\cdot Q(V_i,i)\,dm \tag{29}$$

where dm = fraction of the CR between l/L and $(l+dl)/L$; $dm=2(l/L)\,d(l/L)$. Then from Eqs. (25, 27, and 28),

$$\text{MLF}=1.109\times 10^{-3}(V_i^2/V_{BL})^2\int_0^l\left(\frac{L}{l}\right)\times\left[1+2\left(\frac{l}{L}\right)\right]^2 d\left(\frac{l}{L}\right) \tag{30}$$

The logarithmic term is dealt with by taking the lower limit of integration as $l/L=0.05$. Then, approximately, MLF $=10^{-2}(V_i^2/V_{BL})$. Then if MLF may be as high as 0.01, for $V_i=0.22$ (Fig. 9), $V_{BL}=0.0484=49.5$ m/s. With $R=50$ m, the bag rotates at 10 rpm, producing 5 g's at $l=L$.

Let the bag be constructed of Kevlar and let it be stressed to a safety factor of 2, when full. The yield strength of Kevlar is 3.7×10^9 Pa (525,000 psi) and its density is 1.45 g/cm^3.[10] So for $R=50$ m, $L=150$ m, and for 10^5 tons of CR, the bag's maximum thickness is 1.09 cm and it tapers as l^2. Its mass is then 132 tons.

In summary, there is the following provisional mass budget (in tons): powerplant – 1096, tankage – 47, thrustor systems – 69, bag – 132, total – 1344; propellant is 4713 and ancillary structures and systems may aggregate 100. Then the catcher at t_0 has a total mass of 6157 tons and the value $m_f/m_0=16.24$ is appropriate.

Conclusions

This study has examined whether it is reasonable to propose that a mass-catcher can maneuver so as to always be reached via achromatic trajectories. The answer is in the affirmative. Moreover, optimal catcher trajectories, constructed under this requirement, offer the advantage of modest propellant requirements and initially low impact velocities. The catcher design may be driven by containment requirements rather than by a need to be large enough to intercept a dispersed mass-stream, since low dispersion appears achievable. Mass-catcher power requirements are some 25 MW for a catching rate of 10^5 tons per month. Empty catcher mass is <1500 tons.

This study has also shown how geological data on impact cratering can be used in designing the mass-catcher. But there is need for data at impact velocities of ≤ 250 m/s, such as do not now exist.

The theory of achromatic trajectories provides a unifying framework within which the problem of mass-catching is completely solvable, the solutions leading directly to definition of mass-catcher systems requirements. Hence, this mode of lunar mass transport appears valid and may merit serious attention for any long-range program of space industrialization.

Acknowledgments

This work has benefitted substantially from discussions with William F. Powers and with Herbert A. Zook. This work was supported through a research foundation with the Alexander von Humboldt Foundation, Bonn, West Germany, and represents one phase of research conducted at the Max-Planck-Institut für Kernphysik, Heidelberg.

References

[1] Johnson, R. D. and Holbrow, C. (eds.), *Space Settlements, A Design Study*, NASA SP-413, 1977.

[2] Heppenheimer, T. A. and Kaplan, D., "Guidance and Trajectory Considerations in Lunar Mass Transportation," *AIAA Journal*, Vol. 15, April 1977, pp. 518-525.

[3] Heppenheimer, T. A., "Achromatic Trajectories and Lunar Mass Transport for Space Colonization," *Journal of Spacecraft and Rockets*, Vol. 15, May-June 1978, pp. 176-183.

[4] "Final Report for Lunar Libration Point Flight Dynamics Study," General Electric Co., Contract NAS-5-11551, April 1969.

[5] Heppenheimer, T. A., "Steps Toward Space Colonization: Colony Location and Transfer Trajectories," *Journal of Spacecraft and Rockets*, Vol. 15, Sept.-Oct. 1978, in press.

[6] Chilton, F., Hibbs, B., Kolm, H., O'Neill, G. K., and Phillips, J., "Mass-Driver Applications," in *Space Manufacturing from Non-terrestrial Materials*, edited by G. K. O'Neill, Progress in Aeronautics and Astronautics, Vol. 57, AIAA, New York, 1977.

[7] Marcus, A. H., "Speculations on Mass Loss by Meteoroid Impact and Formation of the Planets," *Icarus*, Vol. 11, July 1969, pp. 76-87.

[8] Overbeck, V. R., Quaide, W. L., Mahan, M., and Paulson, J., "Monte Carlo Calculations of Lunar Regolith Thickness Distributions," *Icarus*, Vol. 19, May 1973, pp. 87-107.

[9] Murray, B. C., "Mercury," *Scientific American*, Vol. 233, Sept. 1975, pp. 58-68.

[10] Commercial data, Dupont de Nemours Corporation, 1975.